NRC Publications Archive
Archives des publications du CNRC

DMFC electrode preparation, performance and proton conductivity measurements

Birry, L.; Bock, C.; Xue, X.; McMillan, R.; MacDougall, B.

This publication could be one of several versions: author's original, accepted manuscript or the publisher's version. / La version de cette publication peut être l'une des suivantes : la version prépublication de l'auteur, la version acceptée du manuscrit ou la version de l'éditeur.
For the publisher's version, please access the DOI link below./ Pour consulter la version de l'éditeur, utilisez le lien DOI ci-dessous.

Publisher's version / Version de l'éditeur:
https://doi.org/10.1007/s10800-008-9678-0
Journal of Applied Electrochemistry, 39, 3, pp. 347-360, 2008-10-28

NRC Publications Record / Notice d'Archives des publications de CNRC:
https://nrc-publications.canada.ca/eng/view/object/?id=a6ece81c-77ec-441c-a95b-f79068f8247d
https://publications-cnrc.canada.ca/fra/voir/objet/?id=a6ece81c-77ec-441c-a95b-f79068f8247d

Access and use of this website and the material on it are subject to the Terms and Conditions set forth at
https://nrc-publications.canada.ca/eng/copyright
READ THESE TERMS AND CONDITIONS CAREFULLY BEFORE USING THIS WEBSITE.

L'accès à ce site Web et l'utilisation de son contenu sont assujettis aux conditions présentées dans le site
https://publications-cnrc.canada.ca/fra/droits
LISEZ CES CONDITIONS ATTENTIVEMENT AVANT D'UTILISER CE SITE WEB.

Questions? Contact the NRC Publications Archive team at PublicationsArchive-ArchivesPublications@nrc-cnrc.gc.ca. If you wish to email the authors directly, please see the first page of the publication for their contact information.

Vous avez des questions? Nous pouvons vous aider. Pour communiquer directement avec un auteur, consultez la première page de la revue dans laquelle son article a été publié afin de trouver ses coordonnées. Si vous n'arrivez pas à les repérer, communiquez avec nous à PublicationsArchive-ArchivesPublications@nrc-cnrc.gc.ca.

National Research Council Canada
Conseil national de recherches Canada
Canada

J Appl Electrochem (2009) 39:347–360
DOI 10.1007/s10800-008-9678-0

ORIGINAL PAPER

DMFC electrode preparation, performance and proton conductivity measurements

L. Birry · C. Bock · X. Xue · R. McMillan · B. MacDougall

Received: 13 March 2008 / Accepted: 1 October 2008 / Published online: 28 October 2008
© National Research Council Canada 2008

Abstract A method that involves stenciling electrodes using dry powders for fuel cells is described and compared to anodes and cathodes prepared by the traditional spraying method using catalyst inks. Methods to determine the proton conductivity of the DMFC anode layer are also discussed. The stenciling method allows for the preparation of highly reproducible membrane electrode assemblies (MEAs) utilizing little waste material. MEAs can be prepared in a controlled manner using the stenciling technique. The resulting morphology of the as-prepared electrodes is observed to be dependent on the preparation method, while the thickness of the once hot-pressed catalyst layers appears to be independent of the preparation method. Stenciled anodes of the same catalyst loading were found to show a lower proton resistance (R_p) than sprayed anodes. However, the lower R_p value was not sufficient to result in a measurable increase in the performance of a direct methanol fuel cell (DMFC); as in fact, the average steady-state DMFC performance was found to be the same using sprayed or stenciled electrodes. The DMFC performance was found to be strongly dependent on the Nafion content and large increases in the Nafion content were needed to increase the DMFC performance measurably. Even though thick electrodes were prepared in this work, the R_p values of the stenciled anodes were found to be comparable to results reported in the literature for much thinner electrodes made using high metal catalyst loadings on carbon. This observation is most probably due to the higher Nafion content used in this work.

L. Birry · C. Bock (✉) · X. Xue · R. McMillan · B. MacDougall
National Research Council Canada, Montreal Road, Ottawa, ON, Canada K1A 0R6
e-mail: Christina.Bock@nrc.ca

Keywords DMFC · Impedance spectroscopy · Electrode structure · Membrane electrode assembly · Conditioning · Fuel cell electrode preparation · Proton conductivity

1 Introduction

Fuel cells have attracted a lot of attention as alternative sources of power. Direct methanol fuel cells (DMFCs) are very promising for, e.g., portable devices that operate in the 40–60 °C range as well as for higher power ranges, e.g., for light traction units such as forklifts. However, a number of technical challenges need to be overcome in order to make DMFCs viable. Some of these challenges are lowering the noble metal catalyst loading, reducing the methanol crossover from the anode to the cathode and addressing water management issues. The catalyst loadings for DMFCs are presently high for both the anode and the cathode. In the case of the anode, high Pt/Ru catalyst loadings of 1–4 mg per cm^2 are typically used due to the sluggishness of the methanol oxidation reaction. Pt catalyst loadings in excess of 1 mg per cm^2 membrane area are used at the O_2 reduction cathode due to both methanol crossover and slowness of the reduction reaction. Methanol crossover has a number of negative impacts such as loss of anode fuel, increase in the Pt loading needed at the cathode as well as depolarization of the cathode, i.e., a lower power output. Designing new membranes to decrease methanol crossover is one approach to increase the performance of a DMFC. However, Nafion is still the membrane of choice in these systems. The anode and cathode catalyst layer structures themselves can be improved by design and performance optimization. One aspect of this approach centers around the fact that the use of thinner electrodes in

DMFCs is an essential requirement, since proton conductivity and oxygen diffusivity within the porous electrode structures can limit high current density performance. However, in order to accomplish such improvements in a systematic manner, one must first address the issue of control of the electrode structure dictated by the fabrication procedure, reproducible MEA fabrication and conditioning processes.

Typical electrode fabrication techniques utilize catalyst inks. For example, electrodes are often made by pasting, brushing or spraying a catalyst ink on the membrane or a carbon based diffusion layer [1–5]. These techniques involve many important variables, most of which are not reported in their entirety in the literature, as for example, the viscosity of the ink solution and the exact composition of the ink (e.g., the solvent to catalyst powder ratio and ionomer content), the spraying pressure and distance, as well as the air to ink ratio. These application techniques typically result in inconsistencies for large electrode areas and are often manual processes. The latter leads to non-uniformities and inconsistencies, affecting the overall morphology and composition of the catalyst layers. This in turn plays a large role in determining the mass transport and kinetic properties of the electrodes and resulting MEAs.

In addition to spraying, alternative MEA fabrication methods have been investigated. Gottesfeld and co-workers [6] prepared MEAs by a decal method, where appropriate amounts of catalyst inks were applied to a Teflon decal blank and dried at 100 °C. The catalyst layers were subsequently transferred from the blank to the Nafion membrane by hot pressing and sandwiching between carbon papers. However, preparation of the catalyst ink and high temperature transfer processing (160–200 °C) were key factors, which can affect the particle size of the Pt catalysts [7].

Gülzow et al. [8–10] explored the utilization of dry powder catalyst mixtures to fabricate MEAs. This method avoids the use of solvents and drying steps. Dry mixtures consisting of the supported catalyst powders, polytetrafluoroethylene (PTFE) and polymer electrolyte powder were sprayed directly onto the membrane or the gas diffusion layer. This step was followed by hot rolling or hot pressing to improve electrical and ionic contact. Reproducible MEAs were made and tested for H_2/O_2 fuel cells.

In this work, a stenciling method that uses powders consisting of a catalyst/ionomer mixture is explored with the main goal to establish a highly reproducible method that involves little waste material for MEA production on the laboratory scale. The principles are similar to the Gülzow's et al. technique [8–10], as MEA electrodes are fabricated from dry mixtures of catalyst powder and ionomer. The stenciling technique has the advantage that it involves neither expensive nor complicated control equipment and allows parameters such as layer thickness, composition, catalyst and ionomer loadings to be easily controlled. The goal of this study is to establish a reproducible MEA fabrication technique that utilizes little waste material. Electrodes made by the stenciling technique are compared to electrodes made by spraying. DMFC performances are obtained at 40 °C, i.e., for a temperature range relevant to micro-fuel cell applications. The electrodes are characterized for their morphology, electro-active surface area and proton conductivity. Relatively thick anodes and cathodes are investigated in this work with the goal of eventually using the appropriate technique to form thinner and more effective electrodes.

2 Experimental

2.1 Chemicals

Commercially available carbon supported catalysts were used in this work. For the anode, a 20 weight (wt.) % Pt-10 wt.% Ru—HiSPEC 5000 (Alfa Aesar) catalyst was used, while for the cathode a 20 wt.% Pt carbon supported catalyst (Electrochem Inc.) was used. 20 and 5 wt.% Nafion solutions in lower alcohols were purchased from Fluka. The Toray carbon paper supports (TGHP-060, E-Tek Co.) contain 10 wt.% PTFE. A Nafion 117 (Electrochem Inc.) membrane is used. ACS grade chemicals and high resistance (>18 Mohm) water were used.

2.2 Electrodes

Cathodes of 1 mg Pt per cm^2 and anodes of 2 mg Pt + Ru per cm^2 were prepared. The final Nafion content of the electrodes is 30 wt.%, and the catalyst loadings are given per cm^2 membrane area, unless otherwise stated. In this work, the Nafion content in wt.% in the electrode is defined as follows:

$$\text{Nafion content (wt.\%)} = \frac{W_{ion}}{W_{ion} + W_{catal}} \times 100 \qquad (1)$$

where W_{ion} is the weight of the dry ionomer and W_{catal} is the weight of catalyst including metal and carbon support.

2.2.1 Electrode preparation using the stencil method

Figure 1 illustrates the principle steps of the stenciling method. The first step of the stencil method is the attempt to coat and well distribute the catalyst with a thin layer of the proton conductive ionomer. To do this, a freeze dry technique in combination with an ultrasonic probe is used. This step differs from the work done by Gülzow et al. [8, 9]

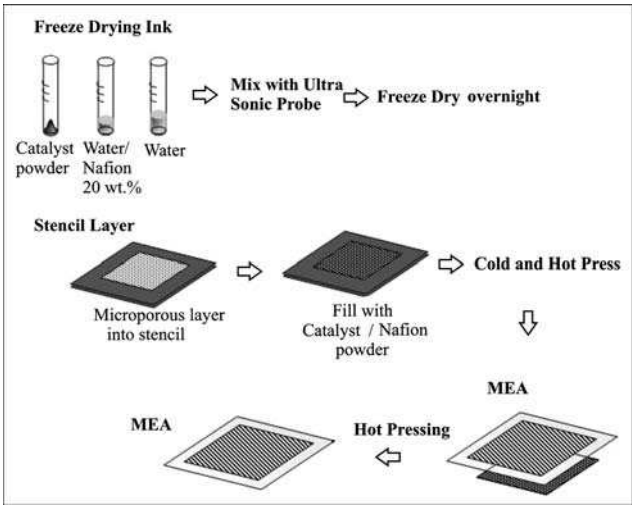

Fig. 1 Scheme showing Membrane Electrode Assembly (MEA) preparation using the stenciling method

who used a knife mill to distribute the catalyst powder and the ionomer. In this work, a known amount of supported catalyst powder is placed into a test tube and an appropriate amount of the 20 wt.% Nafion solution in lower alcohols is added. Subsequently, water is added to achieve a liquid height of ca. 1–2 cm above the catalyst powder. The latter is required for the ultrasonic probe. An ultrasonic probe (Autotune series) is used to mix the ink at an amplitude of 25% for a desired energy (varying between 5 and 40 kJ, requiring between 8 and 60 min., respectively). For the present mixtures (that are all the same, and hence, of the same viscosity), it is estimated that 10 W are applied. The mixture is then placed into a freeze-drying flask (Labconco) and immediately cooled with liquid N_2 to −50 °C. Subsequently, a vaccum is applied at 0.03 mbar and the mixture is slowly dried over a period of 16 h in a FreeZone 1 L Benchtop Freeze Dry System. The mixture is dried by removing the water and alcohols that are collected at the system's trap that is maintained at −50 °C. In order to assists the removal of the solvents, the system is allowed to heat to room temperature (20 °C) over a period of 16 h. The resulting freeze-dried powder is used to stencil the electrodes. A rapid freezing and slow drying process is used in this work, which is expected to form small ice and solvent crystals and a uniform structure of the powder.

An appropriate amount of the freeze dried powder is then placed into a stainless steel stencil and hot pressed at 135 °C for 1 min. at 75 kg cm^{-2} onto a piece of 6.45 cm^2 Toray carbon paper (10 wt.% wet proofed, TGPH-060, E-Tek). The stencil is a mask made out of a flat stainless steel plate exposing an area of 6.45 cm^2. In this work, a stainless steel stencil of 0.99 mm thickness is used. The selection of the thickness is somewhat empirical, but is selected in order to ensure that the stencil provides a sufficient volume to hold the powder. The thickness of the stencil needs to be adjusted if much thinner or thicker electrodes are to be prepared.

2.2.2 *Electrode preparation by spraying*

Catalyst inks were prepared by dispersing appropriate amounts of carbon supported catalyst, water, isopropyl alcohol (IPA), and 5 wt.% Nafion solution in an ultrasonic bath for 1 h. This ink is sprayed onto the Toray carbon paper using an airbrush. The catalyst loading is determined by weighing the carbon paper before and after spraying.

In some cases, electrodes were also prepared by spraying the freeze dried powder. In this case, the ink was prepared by dissolving the freeze dried powder in IPA using an ultrasonic bath for 1 h. Electrodes made by spraying inks made from freeze dried powders or inks made using the as-received catalyst powders were essentially the same, indicating that freeze drying did not have a negative effect on neither the catalyst properties nor the Nafion ionomer.

2.3 Physical characterization: SEM cross-section, anode layer thickness, and BET analysis

Morphology and bulk composition of cross-sections of the as-prepared electrodes were studied by scanning electron microscopy (SEM, JEOL JSM-840A). The unused electrodes were submerged in liquid nitrogen for 30 s and then fractured. This technique is used in an effort to minimize distortion to the electrode. BET surface area data (Micromeritics, ASAP 2000) were collected for freeze-dried catalyst-Nafion powders mixed using different energies using N_2 as adsorption/desorption gas. The anode catalyst layers were also characterized for their BET surface area, pore size and volume. The contribution from the backing layer was found to be negligible.

Catalyst layer thickness measurements were obtained either from SEM cross-sections or using a micrometer (Mitutoyo). Prior to the thickness measurements, the stenciled and the sprayed anodes were hot-pressed once. The thickness of the carbon paper was subtracted from the measurements.

2.4 Electrochemical measurements in solution

The electrodes prepared by the stencil method were cut into pieces of 1 cm^2 geometrical area and placed into a Ti mesh holder. The electrochemical catalyst surface area (A_{cat}) values were estimated by integrating the charge required to oxidize adsorbed CO (CO_{ads}) in 0.5 M H_2SO_4 at room temperature. A_{cat} was obtained using the charge of CO_{ads} (Q_{COads}) and a conversion factor of 420 μC cm^{-2} [11–14],

assuming the oxidation of one monolayer of CO_{ads}. A standard 2 compartment cell, where the working and reference electrode compartments were connected with a Luggin capillary, was employed. A high surface area Pt gauze served as counter electrode. A mercury/mercury sulfate electrode (MSE) served as reference electrode. CO was adsorbed by purging the 0.5 M H_2SO_4 electrolyte solution with CO for 30 min., and subsequently the solution CO was removed by N_2 bubbling for 50 min. The potential was maintained at −0.5 V vs. MSE during the entire process. Two complete cycles between −0.75 and 0.4 V vs. MSE were recorded utilizing a scan rate of 5 mV s^{-1}.

2.5 MEA preparation and single DMFC tests

An anode and cathode were placed on either side of a pretreated Nafion 117 membrane. The membranes were pretreated by boiling (for 1 h in each solution) in 5 wt.% H_2O_2, then in water, in 1 M H_2SO_4, and a second time in water. The membranes were then stored in water. The membrane electrode assembly (MEA) was hot-pressed at 75 kg cm^{-2} for 5 min. at 130 °C. The pressure was maintained for an additional 15 min., while the heating was shut off. The MEA was placed between two graphite current collectors (Electrochem., Inc.) with a serpentine design for the fuel and air distribution, using two silicone gaskets (Electrochem., Inc.) of 0.254 mm thickness exposing 5 cm^2 of MEA area. The temperature of the cell was maintained at 40 °C during DMFC performance testing.

For DMFC performance measurements, a 1 M methanol solution was pumped at 2 mL min^{-1} through the anode side and the cathode side was exposed to dry air at a flow rate of 200 sccm. Fresh methanol solutions were used to collect the individual DMFC performance curves.

2.6 MEA characterization in the DMFC

MEAs were characterized prior to conditioning and collecting DMFC performance curves. A_{cat} [13–15], double layer capacitance (C_{dl}) and proton resistance (R_p) values of the MEAs were obtained in the single cell utilizing the cathode as counter and dynamic hydrogen reference electrode (DHE) [16]. All potentials are referenced vs. the DHE in this work, unless otherwise stated. A_{cat} values were also obtained from CO_{ads} stripping experiments [13–15] carried out in the fuel cell assembly. The electrochemical stripping of the CO_{ads} was preceded by CO adsorption at 0.1 V for 20 min. at 60 sccm of CO gas in a fully humidified cell, followed by purging with N_2 (60 sccm) at 0.1 V for 70 min. to remove non-adsorbed CO. The C_{dl} values of the catalyst layers were extracted from cyclic voltammogramms (CVs) recorded at different sweep rates [17]. The working electrode was fed humidified N_2 (60 sccm) and the cathode humidified H_2 (40 sccm). Using the same gas feeding conditions, R_p values were obtained using electrochemical impedance spectroscopy (EIS) [1, 18–20]. The EIS spectra were collected at constant potentials and at frequencies between 50 kHz and 20 mHz applying a root mean square (RMS) voltage amplitude of 15 mV.

2.7 MEA conditioning and DMFC data acquisition

The MEAs were conditioned at 75 °C by passing 1 M methanol at 2 mL min^{-1} for 2 h at the anode compartment unless otherwise noted. The cathode was exposed to air. The cell was then cooled down to 40 °C for 2 h. Cell polarization curves in the galvanostatic mode were collected using an air flow rate of 200 ccm at the cathode. The influence of using humidified air during DMFC operation at 40 °C was also tested. The DMFC performance was the same with and without air humidification. During the conditioning at 75 °C, a different cathode treatment was tested by feeding the cathode humidified N_2 flow at 150 sccm. Steady-state performance curves obtained immediately after the two conditioning processes were found to be essentially the same, suggesting that there is no need to use humidified N_2 at the cathode during conditioning. In case of impedance testing for proton conductivity measurements, the MEA was conditioned by passing water at the anode and cathode unless otherwise noted.

Anode polarization curves were also collected by passing H_2 (40 sccm) at the cathode. The data reported are obtained after 2 min. at a particular current.

2.8 Electrochemical and DMFC equipment

A Solartron potentiostat 1287 driven by Corrware (Scribner Associates, Inc.) was used to collect all the electrochemical data including the DMFC polarization curves. A Solartron frequency response analyzer 1260 was employed for the EIS measurements. A gas humidification system (Fuel Cell Technologies) was used to humidify the gases for DMFC testing.

3 Results and discussion

3.1 Influence of ink mixing for the anode construction

BET surface area measurements were carried out for freeze-dried powders prepared by mixing the carbon supported Pt-Ru catalyst and the Nafion solution at different energies. As mentioned in the Sect. 2, a rapid cooling and slow drying process was used in this work. The attempt of the entire process is to form a dried powder consisting of

the catalyst and a well-dispersed Nafion ionomer phase. A well dispersed ink is formed by ultrasonically mixing the Nafion ionomer that is dissolved in lower alcohols, and the catalyst powder. Different mixing energies, as indicated in Fig. 2 and the Sect. 2, were used. Immediately after mixing, the ink is rapidly frozen to −50 °C. The rapid freezing used in this work maintains the high dispersion between catalyst powder and ionomer ink. It also forms small ice and solvent crystals that when removed slowly are expected to result in a dry powder consisting of the catalyst and a well dispersed ionomer phase. It is possible that the freeze drying and ultrasonic process used in this work can be further refined to achieve perhaps a higher degree of dispersion of the Nafion ionomer. After freeze drying, the prepared catalyst powders were then placed onto the Toray paper using the stainless steel mask and were hot-pressed. Anodes of 2 mg Pt + Ru per cm^2 loadings were prepared and used to measure the Q_{COads} and A_{cat} values in 0.5 M H_2SO_4 with the three-electrode cell configuration. The goal in this part of the work was to find the optimal energy needed to freeze-dry the catalysts resulting in the highest distribution of Nafion among the catalyst sites. Figure 2 shows the surface area values obtained by BET and CO_{ads} stripping for the various catalyst powders. The BET surface area is for the total weight, i.e., the Pt + Ru + C catalyst including the Nafion, while A_{cat} is calculated per gram of Pt + Ru only. Therefore, the experimental BET and A_{cat} values cannot be directly compared. Both the BET surface area and A_{cat} values show the same trend with the mixing energy. The maximal mixing energy of 40 kJ, applicable with the ultrasonic probe, results in the highest BET and A_{cat} surface area values of 86.5 ± 0.3 and 96.5 ± 3 $m^2\ g^{-1}$, respectively. The values are found to be

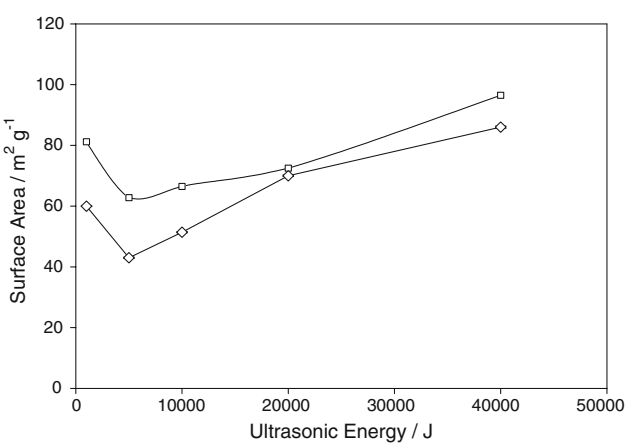

Fig. 2 Surface area for various 20 wt.% Pt + 10 wt.% Ru /C Alfa Aesar catalyst electrodes (with 30 wt.% Nafion content), determined by BET (◇) and CO_{ads} stripping experiments (□) for different ultrasonic mixing energies. The three-electrode arrangement was used for the A_{cat} determination by CO_{ads} stripping

in good agreement with BET data reported in the literature for PtRu/C catalysts [14].

A_{cat} values of sprayed anodes were also obtained. A_{cat} values of 95 ± 5 $m^2\ g^{-1}$ were measured for sprayed anodes, which are comparable to the values obtained for a stenciled anode using the maximal mixing energy of 40 kJ. (For both techniques, the mixing time is almost the same, 1 h.) It is concluded that, in terms of accessible catalyst surface area, electrodes made by freeze drying at 40 kJ and spraying are comparable. The A_{cat} values measured for sprayed and stenciled anodes agree well with the values reported by Guo et al. for brushed 20 wt.% PtRu/C with 30 wt.% Nafion catalysts of 89 $m^2\ g^{-1}$ [21]. Furthermore, the A_{cat} values obtained in 0.5 M H_2SO_4 using three-electrode cell configuration are identical to A_{cat} values obtained in the fuel cell assembly, as shown in Sect. 3.5 and Table 4.

3.2 Anode morphology and thickness

Cross sections of the stenciled and the sprayed anodes were studied using SEM. Figure 3 shows images of as-prepared anodes, both of them hot-pressed. The morphologies of the sprayed vs. stenciled anodes are very different while the thickness is essentially the same, at 90 μm for the two hot-pressed electrodes. The sprayed anode appears compact, but is made of a porous network structure, while the stenciled anode has a layered, flake-like structure. The fact that the thickness of the two hot-pressed anodes is the same could suggest that the porosity (total pore volume) is also independent of the preparation method. However, details of the pores may be different. Additional information about the pore structure of the two electrodes obtained using N_2 adsorption/desorption measurements are discussed below. The N_2 adsorption/desorption method yields information about micropores (<2 nm), mesopores (2–50 nm), and macropores (>50–300 nm) i.e., on a more resolved scale than for the SEM cross-section in Fig. 3.

N_2 adsorption/desorption curves were obtained for the stenciled and sprayed anode catalyst layers. The results are summarized in Table 1. The BET surface area for the carbon paper (as-received and hot-pressed) was also measured and was found to be negligible to the area and pore volumes found for the anode layers. The results in Table 1 are per gram of catalyst layer, which includes the weight of the catalyst, carbon and Nafion. The BET surface area of the stenciled anode is seen to be smaller than for the sprayed anode, which is due to a smaller micropore area for the stenciled anode. In fact, the external surface area, i.e., the area of the meso- and macropores is essentially the same for the two electrodes. The results in Table 1, columns 2 and 3, suggest that 38% of the BET area is made of micropores for the sprayed anode, while 21% of the BET area is made of micropores for the stenciled anode.

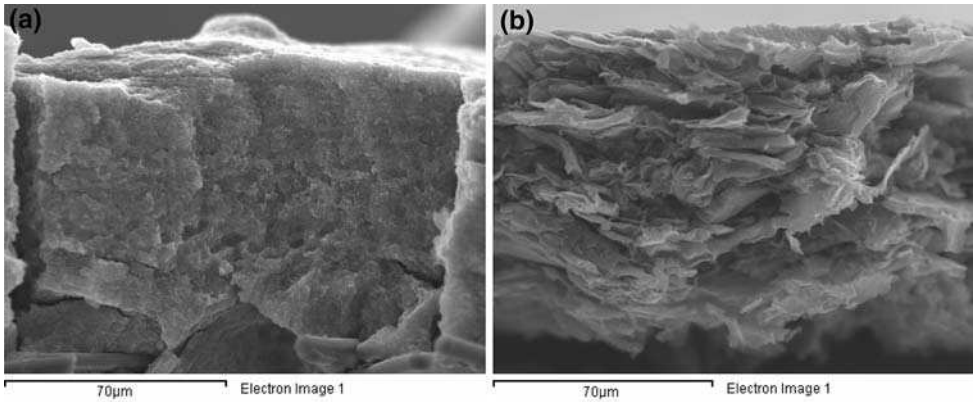

Fig. 3 SEM cross sections of (**a**) sprayed and (**b**) stenciled anodes with loadings of 2 mg Pt + Ru per cm^2 and 30 wt.% Nafion

Table 1 BET surface area and structural parameters determined from N_2 adsorption/desorption isotherms for stenciled and sprayed anodes

Anode	BET S.A./m^2 g^{-1}	Micro-pore A^a/m^2 g^{-1}	External S.A.$^a/m^2$ g^{-1}	Micropore V^a/cm^3 g^{-1}	Mesopore V^b/cm^3 g^{-1}	Macropore V^b/cm^3 g^{-1}	Average pore diameter/nm
Sprayed	42	16	26	7×10^{-2}	8×10^{-2}	1×10^{-1}	34
Stenciled	33	7	26	2.5×10^{-2}	1×10^{-1}	1.1×10^{-1}	34

[a] Micropore (<2 nm) area (A) and volume (V) and external surface area (S.A.) (of >2 nm pores) are obtained from t-plots

[b] Cumulative volumes of mesopores (2–50 nm) and macropores (50–300 nm) are obtained from BJH adsorption and desorption measurements for the sprayed and stenciled anodes. 100% of the pores were set to be open at both ends to yield the same volume for the adsorption and desorption measurements of the two anodes

Consistent with these results, found for the areas per g of anode catalyst layer, the volume of the micropores is larger for the sprayed vs. the stenciled anode, while the volume for the meso-and macropores of the two electrodes are very comparable. It is noteworthy that the volume of the micropores is much smaller than the volume of the meso-and macropores, hence, the difference in the micropore structure of the two electrodes does not add to the total pore volume. The average pore size is estimated to be 34 nm for both electrodes. The average pore size was obtained from BJH adsorption and desorption curves setting the number of pores that are open at both ends to 100% for both samples. The catalysts are likely located in the meso-and macropores of the anodes, rather than the smaller than 2 nm micropores. For both electrodes, the volume and average size of the meso-and macropores are comparable. The meso-and macropores are accessible for water and methanol, which appears to be reflected in the essentially identical A_{cat} values of the two electrodes.

3.3 DMFC performance

3.3.1 Anode: stenciled vs. sprayed

Anodes with loadings of 2 mg Pt + Ru per cm^2 were prepared using the stencil and the spray method. The anodes were conditioned and tested for their DMFC performance, as described in the Sect. 2. All cathodes, with 1 mg Pt per cm^2 loading, were prepared using the stencil method. The steady-state current-voltage characteristics of the MEAs using anodes prepared by stenciling and spraying are obtained in the first day and are presented in Fig. 4. The open-circuit voltage (OCP) of the cell with sprayed and stenciled anodes is slightly higher than 0.6 V, but much lower than the thermodynamic value of 1.2 V [22], indicating that methanol crossover takes place. The DMFC performances obtained with sprayed and stenciled anodes are essentially the same. This indicates that the morphological difference observed by SEM for the as-prepared anodes causes no difference in the performance. It also indicates that the freeze-drying process does not negatively impact the catalysts and the Nafion ionomer. The DMFC performances for different MEAs were found to be reproducible. For example, at a cell voltage of 0.2 V, the current density values were 125 ± 5 mA cm^{-2} (<±5%) using stenciled anodes, while the average current density value was the same, but the reproducibility was lower, namely ±25 mA cm^{-2} (±25%), for sprayed anodes.

3.3.2 Cathode: stenciled vs. sprayed

Cathodes with loadings of 1 mg Pt per cm^2 were prepared using the stencil and the spray method. In all cases, a sprayed anode of 2 mg Pt + Ru per cm^2 was used, thus the anode polarization curves obtained shown in Fig. 5 are the same. The polarization curves using the differently

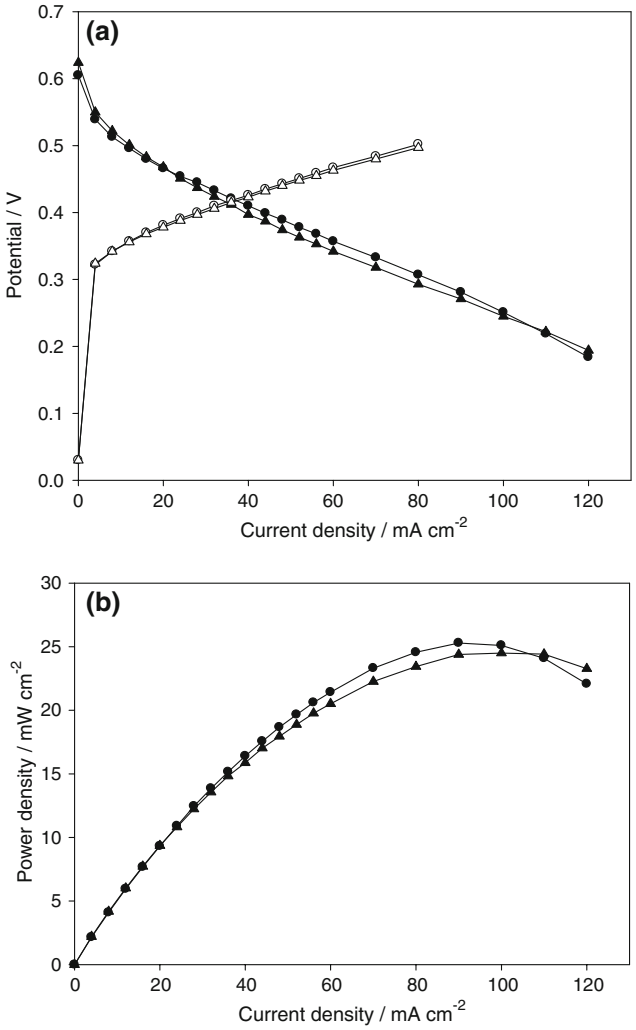

Fig. 4 **a** DMFC steady-state polarization curves at 40 °C for stenciled (-▲-) and sprayed (-●-) anodes (2 mg cm^{-2} of 20 wt.% Pt + 10 wt.% Ru). In all cases, a stenciled cathode (1 mg cm^{-2} of 20 wt.% Pt) was used; The polarization curves were collected flowing 1 M methanol at 2 mL min^{-1} at the anode, and either 200 sccm dry air (Fuel cell mode, filled symbols) or 40 sccm H_2 (anode polarization, open symbols) at the cathode. Steady-state FC performance (cell and anode voltage) was achieved on the first day. **b** DMFC power density curves at 40 °C for stenciled (-▲-) and sprayed (-●-) anodes

prepared cathodes are also shown in Fig. 5. Again, the steady-state cell performances are seen to be essentially the same for both electrodes. The main advantage of the stenciled vs. the sprayed electrodes is that less waste material is produced. Furthermore, the catalyst loading is easier to control with the stencil technique, resulting in higher reproducibility in electrode preparation, hence, the stenciled cathode is used for the further experiments carried out in this work, in which the interest is focused on the anode.

It should be noted that on the laboratory scale tested in this work, the loss of catalyst materials by spraying was 70%, while stenciling results in practically zero loss of

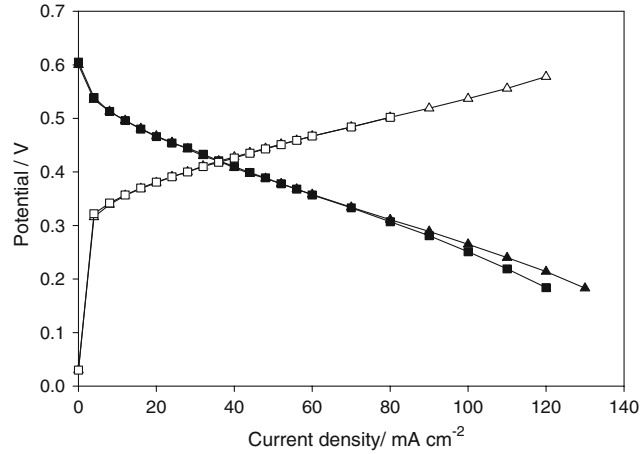

Fig. 5 Steady-state cell polarization curves at 40 °C for sprayed anode (2 mg cm^{-2} of 20 wt.% Pt + 10 wt.% Ru) and either stenciled (-■-) or sprayed (-▲-) cathode (1 mg cm^{-2} of 20 wt.% Pt). The polarization curves were collected flowing 1 M methanol at 2 mL min^{-1} at the anode, and either 200 sccm dry air (Fuel cell mode, filled symbols) or 40 sccm H_2 (anode polarization, open symbols) at the cathode. Steady-state DMFC performance (cell and anode voltage) was achieved on the first day

catalyst waste. The loss of catalyst material on a large scale production using the spray method is lower, but still in the 25% range. Given the fact that the catalyst can contribute between 80 and 90% of the total system cost, a method that involves little or no catalyst waste suggests that a reduction in the 20% range in the system cost is possible. It should be noted that these numbers are estimates. Furthermore, the main intent of the present study was to develop a reproducible method on the laboratory scale. MEAs have been manufactured at a larger scale using dried powders [8, 9]. Nevertheless, further testing is required in order to successfully use this method for large scale production.

3.4 The proton resistance, R_p

3.4.1 Determination of R_p

The aim of this part is to identify an accurate method that allows for the determination of the proton resistance, R_p, in the anode catalyst layer reflecting DMFC operating conditions. The proton conductivity is an important parameter. R_p is of particular importance for DMFCs, where typically high catalyst loadings, and hence thick anodes, are used. In fact, it has been proposed in previous work that less than 7 μm of the DMFC anode [23] is active due to proton conductivity limitations in the catalyst layer. In the case of DMFCs, only a few studies [2, 24] are available, hence, possible measurement procedures for R_p are evaluated and discussed in this work. For PEM fuel cells, the measurement of R_p has been well established [18–20, 25]. The so-called "H_2/N_2 method", combined with ac impedance

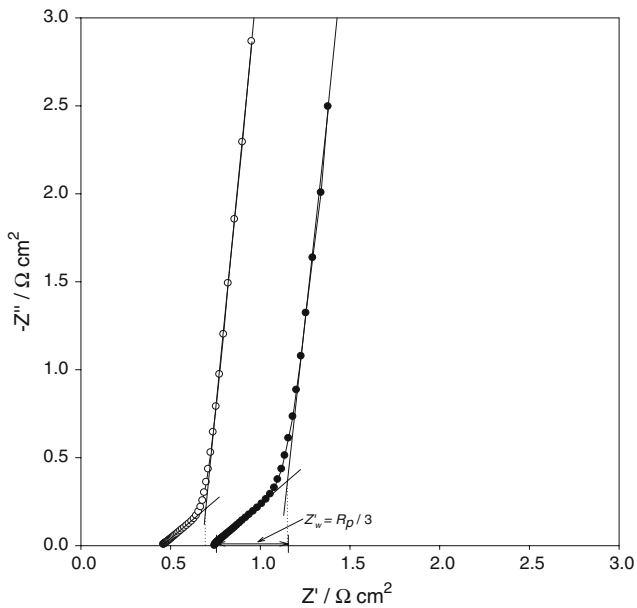

Fig. 6 Nyquist plots obtained for humidified nitrogen-bathed anode (stenciled, 2 mg cm^{-2} of 20 wt.% Pt + 10 wt.% Ru + 30 wt% Nafion) at 0.375 V vs. DHE before (●) and after (○) DMFC performance testing. The MEA is conditioned by passing water and not methanol at the anode (and cathode) prior to the impedance measurements

spectroscopy, is typically used to measure the R_p values in PEM fuel cells. In this method, the catalyst layer of interest is the working electrode and is fed with humidified nitrogen. The other catalyst layer is fed with humidified hydrogen and used as DHE. This method can be used after reaching PEMFC steady-state performance.

The impedance of the catalyst layer is represented by a transmission line [1, 18–20]. An example of Nyquist plots obtained using the "H_2/N_2 method" for MEAs prepared in this work, and used for R_p measurements, is shown in Fig. 6. A Warburg-like response (45° slope) is typically observed at high to intermediate frequencies provided that the catalyst is uniformly distributed within the electrode layer. The Warburg response corresponds to semi-infinite diffusion of protons through the catalyst layer. At lower frequencies, a 90° vertical line is observed, corresponding to the total capacitance and resistance of the catalyst layer. R_p can be obtained from the Warburg impedance. The length of the Warburg region is projected onto the real impedance axis and the high frequency intercept Z′ value is subtracted yielding the Z'_W value. This Z'_W value is related to R_p, as follows [18–20] (see also Fig. 6):

$$Z'_W = \frac{R_p}{3} \tag{2}$$

According to the theory described in [25], R_p can also be determined from the modulus |Z| at a given angular frequency, ω:

$$|Z| = K\omega^{-1/2} = \sqrt{\frac{R_p}{C_{dl}}}\omega^{-1/2} \tag{3}$$

In Eq. 3, C_{dl} is the double layer capacitance, which can be determined from CV experiments, as discussed in Sect. 3.4 b and c and K is the unitless slope of a plot of |Z| vs. $\omega^{-1/2}$. For PEMFCs, before ac impedance measurements using the "H_2/N_2 method" are taken, the cell is usually operated with humidified H_2 on the anode and dry O_2 on the cathode. This is done in a potentiostatic mode until a steady current is obtained. This conditioning process is not applied here in order to avoid any possible deterioration of the MEAs prior to DMFC testing. However, humidification of the catalyst layer is an important factor to allow good proton conductivity and reach steady-state conditions. Hence, another conditioning process is employed in order to test the validity of determining R_p using the "H_2/N_2 method".

3.4.2 R_p values before and after DMFC testing: "The H_2/N_2 method"

The following conditioning process and measuring sequence was adopted in this work in order to measure the R_p, C_{dl} and A_{cat} values before and after the collection of DMFC performance curves. In this process, water is circulated at both the anode and the cathode at 40 °C overnight. Subsequently, excess water is flushed using humidified N_2 at 60 sccm at the anode and humidified H_2 at 40 sccm at the cathode for 15 min. before the measurements of R_p, C_{dl} and A_{cat} are carried out. After these tests, the usual conditioning process at 75 °C for 2 h is repeated and DMFC polarization curves are recorded. The water circulation process is repeated and the measurements of R_p, C_{dl} and A_{cat} are carried out again.

Figure 6 shows the complex plane plots obtained for a conditioned anode prior to and after DMFC curves are obtained. Prior to DMFC testing, the MEA is free of methanol, hence a charge transfer reaction due to methanol oxidation can be ruled out. The impedance spectra are collected at 0.375 V, which is in the double layer region (see below and Fig. 8). A straight line of 41° is observed at high frequencies followed by a line of a ca. 84° slope at low frequencies. The deviation from 90° at low frequencies cannot be explained by a pure capacitance. The use of a constant phase element (CPE) is more appropriate in this case to simulate non-ideal conditions that are typically observed for porous electrodes [26, 27]. Using the graphical method and Eq. 2, an R_p value of 1.18 Ω cm^2 is determined for the stenciled anode prior to DMFC testing. The second method for the R_p determination, i.e., a plot of the modulus of the impedance |Z| in the Warburg region vs. $\omega^{-1/2}$, is shown in Fig. 7. A straight line is obtained with a

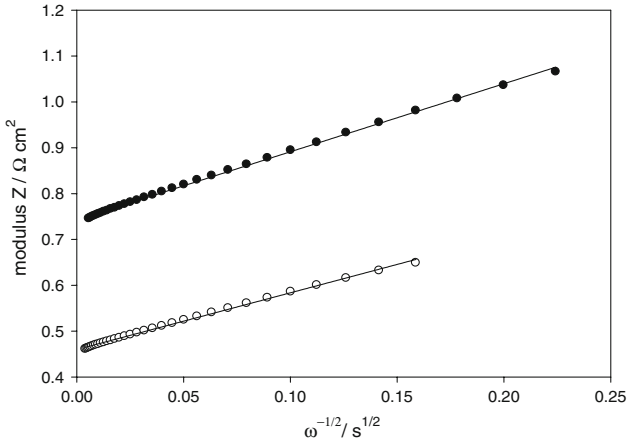

Fig. 7 Modulus of the impedance |Z| plotted vs. $\omega^{-1/2}$. The experimental data are taken from Fig. 6, i.e., before (●) and after (○) DMFC performance curves are obtained. ● shows the data before DMFC testing, the linear regression obtained is: $y = 1.484\,x + 0.743$ ($R^2 = 0.999$). ○ shows the data after DMFC testing, the linear regression is: $y = 1.238\,x + 0.460$ ($R^2 = 0.999$)

slope, K, of 1.484. K equals $\sqrt{\frac{R_p}{C_{dl}}}$, as shown in Eq. 3. To obtain the value C_{dl}, CVs are collected at different scan rates in the double layer region, i.e., between 0.32 and 0.45 V. A C_{dl} value of 479 mF cm^{-2} is extracted from the CV data shown in Fig. 8 utilizing Eq. 4 [17]:

$$\Delta j_{dl} = 2C_{dl}\,v \tag{4}$$

In Eq. 4, $\Delta j_{dl} = j_a - j_c$ is the difference between the anodic and cathodic current density. A plot of Δj_{dl} vs. the scan rate is shown in Fig. 8b. The Δj_{dl} value is seen to increase linearly with the scan rate and pass through a zero intercept, as expected for a capacitive current density. The Δj_{dl} value is found to be independent of the potential range tested, i.e., between 0.32 and 0.45 V. This suggests an R_p value of 1.06 Ω cm^2, which is close to the R_p value of 1.18 Ω cm^2 obtained using the graphical method.

After the collection of steady-state DMFC performance curves, the anode compartment is flushed to remove the methanol fuel by passing water overnight. Subsequently the R_p, C_{dl} and A_{cat} measurements are repeated. The impedance spectrum obtained after collecting the DMFC performance curves are also shown in Figs. 6 and 7. It is seen in Fig. 6 that the high frequency intercept, which corresponds to the sum of the membrane resistance and various electronic contacts and bulk resistances [20], is lower than it was prior to collecting the DMFC performance curves. This is most likely due to an increased humidification of the Nafion membrane [28]. The R_p value is also found to be smaller. This is expected when better anode humidification is achieved. Using the graphical method, an R_p value of 0.69 Ω cm^2 is found. The C_{dl} value determined from CV data is 420 mF cm^{-2}. Furthermore, the slope K is 1.238, thus these results suggest an R_p value

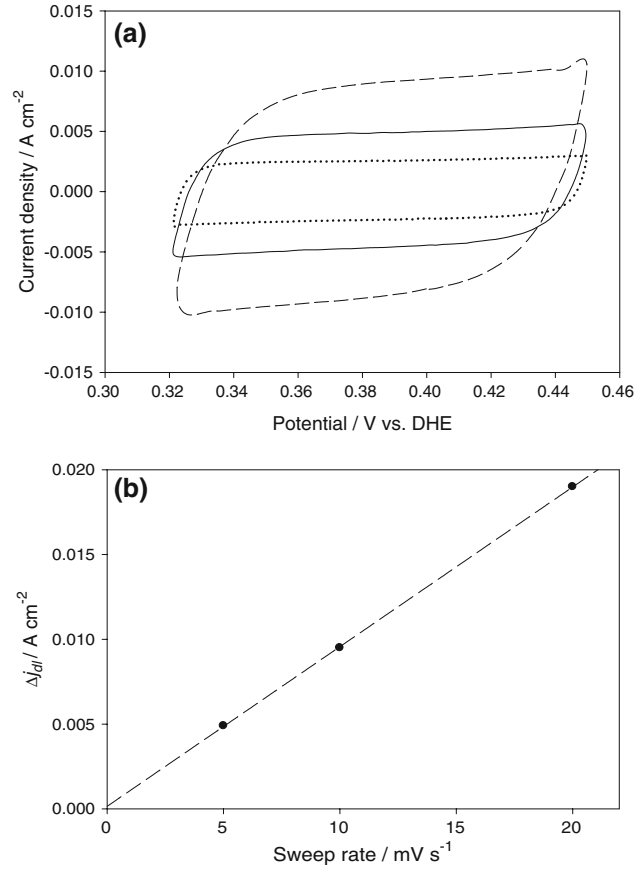

Fig. 8 **a** Typical cyclic voltammograms for a stenciled anode recorded at different sweep rates, 5 (···), 10 (—) and 20 mV s^{-1} (- - -). The same MEA as in Fig. 6 is used for the measurements, which are carried out using the "H_2/N_2 method" and thus the cathode as DHE. **b** Current density Δj_{dl} values measured at 0.375 V as a function of the sweep rate. The Δj_{dl} values are extracted from Fig. 8a, as described in the text

of 0.64 Ω cm^2. All the measured and calculated values are summarized in Table 2. The results suggest a decrease in the R_p value of almost 40% as a result of DMFC testing. This decrease was observed on all the MEAs studied in this work, and is believed to reflect an improvement in the humidification of the anode.

3.4.3 R_p values measured in the presence of methanol

In this case, the MEAs are tested in a driven cell mode using methanol fed to the anode (as working electrode) and hydrogen to the cathode (as DHE and counter electrode). Measurements carried out under these conditions are likely to reflect the R_p value close to real DMFC operating conditions. The impedance measurement can be done after anode steady-state performances are reached. The estimation of C_{dl} is an issue in the presence of methanol. This is seen in Fig. 9 that shows the CV of the anode catalyst layer recorded using 1 M methanol feed. Even at potentials as

Table 2 Examples of data extracted from impedance and CV measurements for a stenciled anode[a]

Parameters[b]	Values	
	Before DMFC testing	After DMFC testing
C_{dl}/mF cm^{-2}	479	420
K	1.484	1.238
R_p from Eq. 2/Ω cm^2	1.18	0.69
R_p from Eq. 3/Ω cm^2	1.06	0.64

[a] The stenciled anode contained 2 mg Pt + Ru per cm^2 membrane area and a Nafion content of 30 wt.%. A commercial, carbon supported 20 wt.% Pt + 10 wt.% Ru catalyst on Vulcan XC-72 is used

[b] Parameters are extracted from experimental data shown in Figs. 6–8. C_{dl} is the double layer capacitance measured from CV curves using different sweep rates, as shown in Fig. 8. K is the slope of a plot of |Z| vs. $\omega^{-1/2}$ as defined in Eq. 3 and R_p is the proton resistance of the anode measured at 0.35 V using the "H_2/N_2 method"

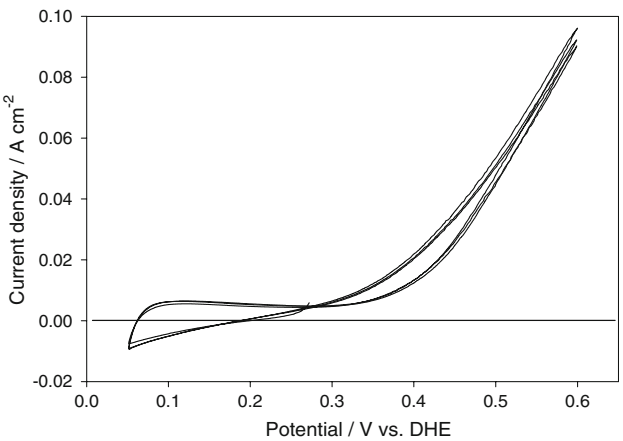

Fig. 9 Cyclic voltammograms (3 cycles) recorded at 10 mV s^{-1} for an MEA made using a sprayed anode (2 mg cm^{-2} of 20 wt.% Pt + 10 wt.% Ru) and a stenciled cathode (1 mg cm^{-2} 20 wt.% Pt). 1 M methanol at 2 mL min^{-1} at the anode, 40 sccm H_2 at the cathode

low as 0.25 V, a positive current due to methanol oxidation is observed. At more negative potentials, adsorption of atomic H and CH_3OH takes place. Hence, in the presence of methanol there is no double-layer only region. A potential of 0.25 V is used in this work as a compromise to measure a "pseudo-C_{dl}" value. To avoid faradaic processes, in the present case methanol oxidation, the ac spectra must also be recorded at low potentials, where methanol oxidation kinetics are slow. Again, CVs at different scan rates were recorded, however, in the potential range of 0.14 and 0.3 V, as shown in Fig. 10a. At 0.25 V, the current density increases linearly with the scan rate, as predicted by Eq. 4 and shown in Fig. 10b. This "pseudo-C_{dl} value" is smaller than the one obtained using the "H_2/N_2 method" due to the contribution of adsorbed methanol at 0.25 V.

AC spectra in the presence of methanol were recorded at 0.25 V. The high frequency range is chosen to minimize

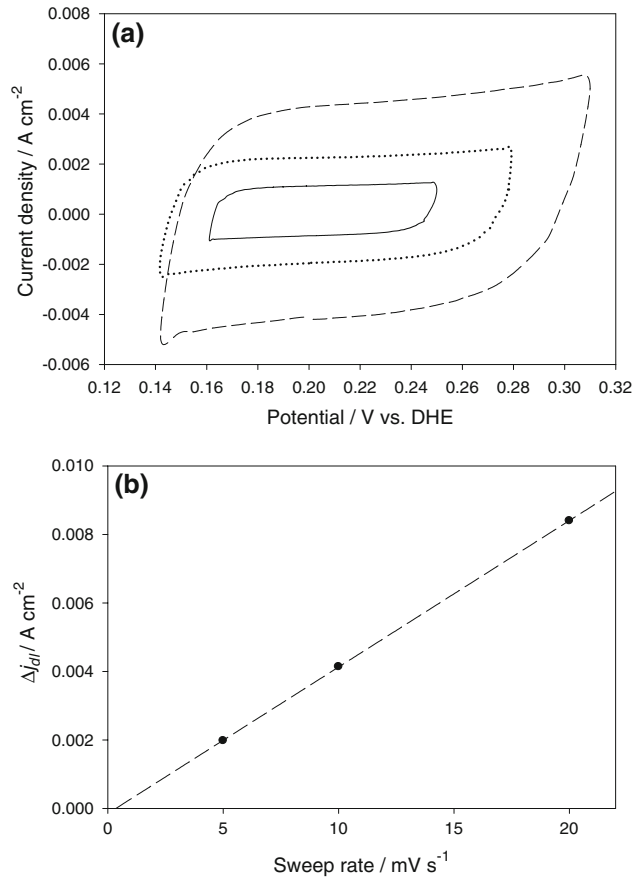

Fig. 10 (**a**) Typical cyclic voltammograms recorded at different sweep rate, 5 (—), 10 (···) and 20 mV s^{-1} (- - -). (**b**) Current density Δj_{dl} measured at 0.22 V as a function of the sweep rate. Same MEA and conditions as in Fig. 9

influences of faradaic processes on |Z|. The R_p value obtained in the presence of methanol and using the graphical method is 0.7 Ω cm^2. This value is very similar to the values obtained using the "H_2/N_2 method" after DMFC performance testing, thus validating this measurement procedure in the presence of methanol. It is concluded that either method, i.e., the "H_2/N_2 method" used after DMFC testing or the measurements in the driven cell mode in the presence of methanol at 0.25 V vs. DHE, are appropriate to obtain the R_p value of these anodes. All additional R_p values reported in this work are measured after DMFC testing using the "H_2/N_2 method".

3.4.4 R_p and σ_p values for stenciled vs. sprayed anodes

In this section, the R_p values for both stenciled and sprayed anodes of the same composition, namely 2 mg Pt + Ru per cm^2 and 30 wt.% Nafion content, are measured and compared. For each preparation method, 5 anodes were prepared and studied. For the stenciled anodes R_p values of 0.73 ± 0.03 Ω cm^2 were determined. The deviation from

anode to anode is seen to be very small indicating that the stenciling method allows for very reproducible catalyst layer preparation. In the case of the sprayed anodes, larger variations in the R_p values were found. Furthermore, the R_p values are found to be 40% larger, namely $1.02 \pm 0.17\ \Omega\ cm^2$, than the values determined for stenciled anodes. Despite the 40% difference in the R_p values, very similar DMFC steady-state performances were observed for MEAs made using either stenciled or sprayed anodes. Hence, additional experiments need to be carried out to determine the limiting factors for the DMFC performance, as further discussed in Sect. 3.5. The low variation in the R_p value for stenciled anodes vs. the larger variation for sprayed anodes is consistent with the variation in the DMFC performance, as shown in the j values at 0.2 V cell voltage that are also listed in Table 3. Again, this highlights the high reproducibility of the stencil method. The R_p values are comparable to values reported by Havránek and Wippermann [24]; examples of the latter are also listed in Table 3. In their work, R_p was determined for sprayed anodes that were made of high Pt/Ru loadings (84–95 wt.%) on carbon black and for different Nafion contents in the 5–16 wt.% range. In the latter case, the anode layer thickness is much thinner than in our work, namely ~10 vs. ~100 μm; however, the R_p value of the latter is not smaller. This is assigned to the fact that a higher Nafion content is used in this work, thus providing a more continuous network for proton transport (see Sect. 3.5).

The proton conductivity, σ_p, value in the anode catalyst layer is related to R_p and the thickness, d_a, of the anode catalyst layer, as follows:

$$\sigma_p = \frac{d_a}{R_p} \tag{5}$$

The thicknesses of stenciled and sprayed anodes prepared in this work that consist of 2 mg Pt + Ru per cm^2 and 30 wt.% Nafion are listed in Table 3. The values shown in Table 3 are measured using a micrometer, as described in the Sect. 2. The values are for as-prepared electrodes. They may not reflect the correct value of the anode layer when steady-state DMFC performance is reached and the R_p values are measured. However, these values are used here, as cross-sectioning of used MEAs, and hence anode layer thickness measurements, are difficult due to their brittleness. The σ_p values are calculated using Eq. 5. Table 3 also shows literature σ_p values for comparison. σ_p values of 12 and 9 mS cm^{-1} for the stenciled and sprayed anodes, respectively are estimated. The σ_p values are one order of magnitude lower than found for bulk Nafion, which is reported as 120 mS cm^{-1} at 40 °C [24]. As discussed in previous work, this difference can be explained by the tortuosity of the Nafion phase in the catalyst layer [29].

3.5 Effect of the Nafion content in the anode on DMFC performance

The influence of the ionomer content in the catalysts layers on the DMFC performance has been studied for carbon supported [30] and unsupported [2, 30, 31] Pt-Ru catalysts. The performance of a DMFC is dependent on the Nafion content. Optimal contents have been determined for supported and unsupported catalysts. At low contents, the proton conductivity in the catalyst layer increases with increasing Nafion content. However, at high ionomer contents the Nafion can block catalyst sites and introduce mass transport limitations of the methanol fuel into the electrodes of increased thickness [31]. A limitation to catalyst utilization due to a poor electronic conductivity is also possible to explain a decrease of the performance at high ionomer contents. Sasikumar et al. [32] have shown that for H_2 fuel cells, the optimal ionomer content depends on the catalyst loading. The goal of this present part is not

Table 3 Comparison of various parameters of sprayed and stenciled anodes as well as literature data

Sample	d_a/μm	R_p/ohm cm^2	σ_p/mS cm^{-1}	j^f/mA cm^{-2}
Sprayed anode[a] (30 wt.%Nafion)	91 ± 15[c]	1.02 ± 0.2[d]	9[e]	125 ± 25
Stenciled anode[a] (30 wt.%Nafion)	89 ± 5[c]	0.73 ± 0.03[d]	12[e]	125 ± 5
Sprayed anode [24][b] (16 wt.%Nafion)	11	0.42	2.6	
Sprayed anode [24][b] (10 wt.%Nafion)	13	1.34	1	

[a] Anodes prepared in this work. They consist of 2 mg Pt + Ru per cm^{-2} membrane area and are made using 20 wt.% Pt + 10 wt.% Ru on carbon black

[b] Values taken from Ref. [24]. The R_p and d_a values are recalculated for the 2 mg PtRu cm^{-2} loadings used in this work. A 84–95 wt.% Pt + Ru anode catalyst on carbon black was used

[c] Thickness of the anode catalyst layer measured using a micrometer prior to hot-pressing the MEA assembly. Both anode catalyst layers are hot-pressed once. The thickness of the carbon paper, 200 μm, is subtracted

[d] Values measured using the "H_2/N_2 method" at 0.375 V vs. DHE

[e] The σ_p values are calculated using the mean values of R_p and d_a values listed in the Table and Eq. 5

[f] Current density of a single cell DMFC at 0.2 V cell potential, 1 M methanol feed and 40 °C cell temperature

Table 4 The influence of the Nafion content on various anode parameters

Nafion content[a]/wt.%	d_a[b]/μm	Vol% Nafion[c]/%	A^d_{cat}/m^2 g^{-1}	R^e_p/ohm cm^2	n[f]
15	80 ± 15	8	95	8.3	1.9
30	91 ± 15	17.5	100	1	1.5
40	93 ± 15	27.5	100	0.3	1.3
50	112 ± 15	33	95	~0.1–0.15	0.06–0.42

[a] Nafion content of the anode catalyst layer, as defined in Eq. 1. All anodes are made by spraying and are of 2 mg Pt + Ru per cm^2 loading

[b] Thickness of the resulting anode catalyst layer (d_a). The anode layer is hot-pressed prior to the measurement. The thickness of the carbon paper backing, 200 μm, is subtracted

[c] Volume percentage of Nafion in the anode layer. The value was calculated using a Nafion density of 1.8 g cm^{-3} and the anode thickness, d_a listed in column 2 in Table 4

[d] Surface area, A_{cat}, measured from experimental CO_{ads} stripping voltammograms in the fuel cell assembly. The values are per g of Pt + Ru

[e] R_p values measured at 0.375 V vs. DHE using the "H_2/N_2 method"

[f] The exponent n is calculated using the R_p and d_a values listed in Table 4 and eqs. 5+6. The n value relates to the microstructure and tortuosity of the Nafion phase

to find the optimal Nafion content for our carbon supported Pt-Ru catalyst layers, but to check how the increase in Nafion content influences the surface area and the proton conductivity as well as the DMFC performance.

Anodes with loadings of 2 mg Pt + Ru per cm^2, but with different Nafion contents, were prepared using the spray method. The spray method was used to prepare the different anodes since the freeze drying involved in the stenciling method requires the preparation of "large" batches (several grams) of catalyst-ionomer powders. All cathodes, of 1 mg Pt per cm^2 and 30 wt.% Nafion loadings, were prepared using the stencil method. The thicknesses of the anode catalyst layers were also measured and are reported in Table 4. The thickness increases with Nafion content, however, the increase is not pronounced. This suggests a strong increase in the volume fraction of Nafion in the catalyst layer, which is expected to be accompanied by a decrease in the porosity of the catalyst layer. The calculated values for the volume % (Vol.%) of Nafion in the catalyst layer are also shown in Table 4. The values were calculated using the d_a values listed in Table 4 and a density for Nafion of 1.8 g cm^{-3}. Based on these calculations, the Vol.% of Nafion in the catalyst layer is suggested to increase by a factor of 4 with an increase in the Nafion content from 15 to 50 wt.%. This in turn enhances the proton conductivity of the anode catalyst layer drastically, which is indeed observed in the decrease of the R_p values also listed in Table 4. The catalyst surface area is not significantly influenced by the change in the Nafion content. However, the improved proton conductivity of the anode layer results in a significant increase in the DMFC performance shown in Fig. 11.

The increase in Nafion content has a large impact on R_p. The R_p values decrease from 8 to 0.1 Ω cm^2 upon increasing the Nafion content from 15 to 50 wt.%. These results explain why the difference in R_p between sprayed

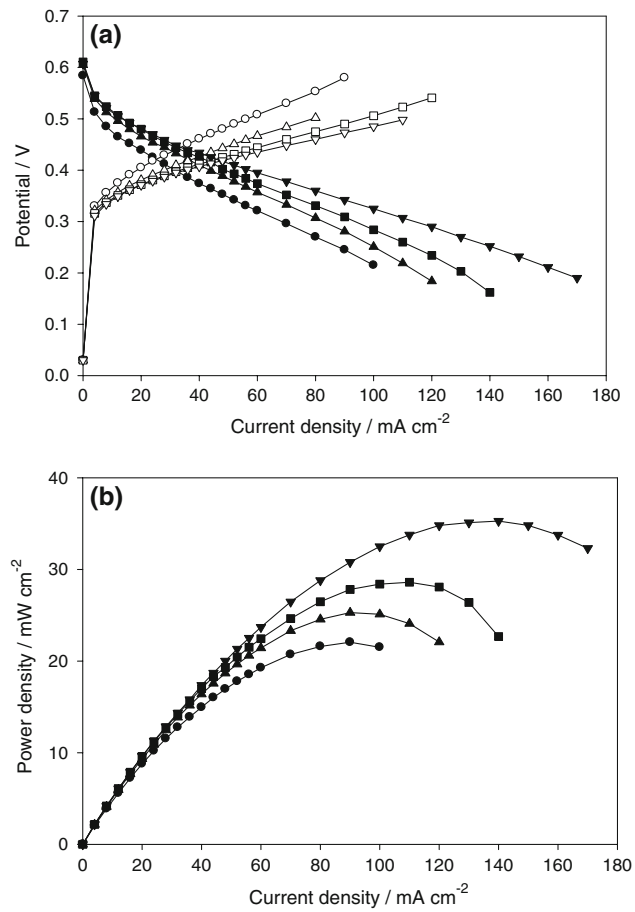

Fig. 11 (**a**) DMFC steady-state polarization curves and (**b**) DMFC power density curves at 40 °C for sprayed anodes (2 mg cm^{-2} of 20 wt.% Pt + 10 wt.% Ru) with 15 (●), 30 (▲), 40 (■) and 50 wt.% (▼) of Nafion content. In all cases, a stenciled cathode (1 mg cm^{-2} of 20 wt.% Pt) was used. The polarization curves were collected flowing 1 M methanol at 2 mL min^{-1} at the anode, and either 200 sccm dry air (Fuel cell mode, filled symbols) or 40 sccm H_2 (anode polarization, open symbols) at the cathode. Steady-state FC performance (cell and anode voltage) was achieved on the first day

and stenciled anodes, of ca. 30%, does not influence the DMFC performance. A bigger difference is needed to have a significant impact on the DMFC performance.

A further increase in the Nafion content of the anode may further increase the DMFC performance. For example, for a DMFC anode with 3 mg of PtRu (53.3 wt.% PtRu/C) per cm^2, the optimal Nafion content was reported as 60 wt.% [30]. Our catalyst loading on carbon being lower, and thus our catalyst layer thickness being more important, the optimal Nafion content may be even higher than 60 wt.%. However, future work will focus on using higher PtRu on carbon loadings, which should allow for the preparation of thinner electrodes, and hence better catalyst utilization. Therefore, the low catalyst on carbon loading layers used here were not further optimized.

Figure 12 shows a plot of the proton conductivity (σ_p) vs. the Vol.% of Nafion. A similar plot has been presented by Havránek et al. [24] for MEA anodes made of unsupported catalysts and by Boyer et al. [29]. Similar to Havránek et al., the relationship between σ_p vs. the Vol.% of Nafion obtained for these electrodes is not linear. The σ_p values at low Vol.% of Nafion (e.g., 1 mS cm^{-1} at 8 Vol.%) are comparable to the values obtained by Havránek et al. [24]. The influence of lower Vol.% amounts of Nafion onto the proton conductivity was not tested, as the Vol.% of Nafion of less than 8 was too small to make a mechanically stable electrode. The σ_p values and the following empirical equation were used to obtain more information about the micro-structure and tortuosity of the Nafion phase [29]:

$$\sigma_p = \varepsilon^n \sigma_{bulk,Nafion} \quad (6)$$

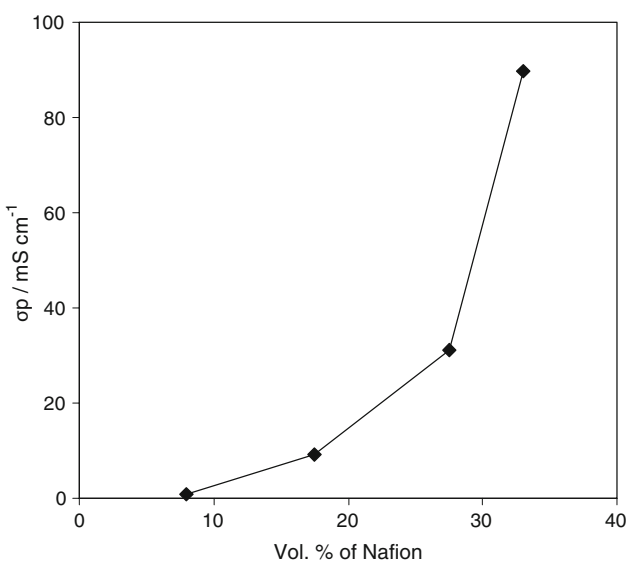

Fig. 12 Plot of σ_p vs. the Vol.% of Nafion for a sprayed anode. The σ_p values are determined using the R_p and d_a values listed in Table 4 and using Eq. 5

In Eq. 6, ε is the volume fraction of Nafion and $\sigma_{bulk,\ Nafion}$ is the specific proton conductivity of bulk Nafion, which is 0.1 S cm^{-1} at 25 °C. n is the exponent that is calculated. The n value depends on the microstructure and tortuosity of the Nafion phase. The n values estimated in this manner are listed in Table 4. Typical n values range from 1.2 to 4.5 [24, 29], i.e., the values for the 10–40 wt.% (i.e., 8–28 Vol.%) Nafion are well within the typical range observed. An n value of unity indicates a phase of no tortuosity. The n value for the 50 wt.% Nafion is estimated to be less than unity. It should be noted the error in the (very small) R_p value is large, and hence, the accuracy of the estimated n value is questionable. One can also expect that for very high weight and volume fractions, the Nafion starts to form a bulk phase of no or low tortuosity. In any case, the n value for the 50 wt.% Nafion electrode is questionable. The n value for the stenciled anode (30 wt.%) was estimated to be 1.3, i.e., well within the expected range. Our n values are comparable to the value of 1.5 often set for FC electrodes.

4 Conclusions

In this work, electrodes for DMFCs are fabricated and compared using a stenciling and the well known spraying technique. The prepared MEAs are tested for DMFC performance at 40 °C and characterized for the electrode active catalyst surface area, as well as proton conductivity of the anode, and the anode layer thickness. The stenciling technique is found to be able to give highly reproducible MEAs, as seen in the low variance (<5%) of the DMFC performances at a particular cell voltage vs. the up-to 25% variance for sprayed anodes. Similarly, the proton resistance values of anode layers made by stenciling are also within 5%, while the variance for sprayed anodes is again larger, namely up-to 25%. The stenciling technique is convenient as it utilizes dry powders and it produces little waste material. The morphologies of the as-prepared anodes in the micrometer scale observed by SEM are found to be significantly different using the spraying vs. the stenciling technique, while the thickness of the as-prepared, and one time hot-pressed anode catalyst layers, is essentially the same. N_2 adsorption/desorption measurements further suggest that the sprayed anodes have a larger micropore (<2 nm) area and volume, while the volume and average pore size for the meso- (2–50 nm) and macropores (50–300 nm) are very comparable for sprayed and stenciled anodes. The morphological differences observed in the SEM and the micropore area and volume of the as-prepared anodes does not influence the DMFC performance, as essentially the same (within the experimental error) DMFC performances are obtained using sprayed and stenciled

anodes. Electrodes were manufactured and investigated on a laboratory scale and the majority of the measurements were carried out overall several days. However, it was confirmed in parallel work that MEA's can be made using both techniques that lasted for over 2,000 h of DMFC operation.

In this work, methods and measurement sequences for the determination of the proton resistance, R_p, of the anode catalyst layer of the DMFCs are also tested. Measurements in the presence and absence of methanol in the catalyst layer were carried out. It was found that both methods yield the same results provided that the appropriate experimental conditions are used. In the presence of methanol, R_p was determined at low potentials in order to minimize the contribution of the methanol oxidation current. Measurements without methanol feed were carried out using the "H_2/N_2 method" typically employed for PEMFCs. In this method, the anode is fed with humidified N_2, while H_2 feed serves to utilize the cathode also as dynamic reference electrode. Humidification of the ionomer in the catalyst layer is a critical issue in obtaining steady-state and reproducible R_p measurements, particularly when the "H_2/N_2 method" is used. It is necessary to obtain steady-state DMFC performance curves, and then carry out the R_p measurements. The proton conductivity, σ_p, of the anode layer is estimated to be 12 ± 0.5 mS cm^{-1}, and 9 ± 1.5 mS cm^{-1} for stenciled and sprayed anodes, respectively, that are made of 30 wt.% Nafion. These values agree with the measurements of Havránek and Wippermann [24], who obtained proton conductivity values of the same order of magnitude for sprayed anodes. The proton conductivity is ca. 30% higher for stenciled vs. sprayed anodes. However, this difference is too small to influence the DMFC performance measurably. In fact, studies using anodes made of different Nafion contents carried out in this work indicate that large increases in the Nafion content are needed to improve the DMFC performance. For the 2 mg Pt + Ru per cm^2 membrane area anode loadings used in this work (that are made of commercial 20 wt.% Pt and 10 wt.% Ru on carbon black), a decrease in R_p from 8 to 0.1 Ω cm^2 was achieved by increasing the Nafion content from 15 to 50 wt.%. This resulted in a 1.6 times increase in the maximal power density of a single DMFC. The use of higher Nafion contents did not increase the anode layer thickness drastically. Therefore, the Vol.% of Nafion in the anode layer increased by a factor of 4, thus providing a more continuous network for proton transport in the anode layer. It appears that the increase in Vol.%. Nafion, and the accompanied lowering of R_p, is mainly responsible for the observed increase in the maximal power density.

Acknowledgements The authors thank D. Kingston (NRC, Ottawa) for the cross-sectioning of the catalyst layers and the SEM images, and R. G. Allen and S. Argue (NRC, Ottawa) for the BET analysis. Financial support from NRC-NSC-ITRI and NRC's Horizontal Fuel Cell program is also gratefully acknowledged.

References

1. Xie Z, Navessin T, Shi K, Chow R, Wang Q, Song D, Andreaus B, Eikerling M, Liu Z, Holdcroft S (2005) J Eletrochem Soc 152:A1171
2. Zhao X, Fan X, Wang S, Yang S, Yin B, Xin Q, Sun G (2005) Int J Hydrogen Energy 30:1003
3. Seiler T, Savinova ER, Friedrich KA, Stimming U (2004) Electrochim Acta 49:3927
4. Lindermeir A, Rosenthal G, Kunz U, Hoffmann U (2004) J Power Sources 129:180
5. Frey T, Linardi M (2004) Electrochim Acta 50:99
6. Ren X, Wilson MS, Gottesfeld S (1996) J Electrochem Soc 143:L12
7. Song SQ, Liang ZX, Zhou WJ, Sun GQ, Xin Q, Stergiopoulos V, Tsiakaras P (2001) J Power Sources 145:495
8. Gülzow E, Schulze M, Wagner N, Kaz T, Reissner R, Steinhilber G, Schneider A (2000) J Power Sources 86:352
9. Gülzow E, Kaz T, Reissner R, Schilling L, Bradke MV (2002) J Power Sources 105:261
10. Gülzow E, Kaz T (2002) J Power Sources 106:122
11. Bock C, MacDougall B, LePage Y (2004) J Electrochem Soc 151:A1269
12. Bock C, Blakely M–A, MacDougall B (2005) Electrochim Acta 50:2401
13. Gasteiger HA, Markovic N, Ross PN, Cairns EJ Jr (1994) J Phys Chem 98:617
14. Dinh HN, Ren XF, Garzon H, Zelenay P, Gottesfeld S (2000) J Electroanal Chem 491:222
15. Roth C, Martz N, Hahn F, Léger J-M, Lamy C, Fuess H (2002) J Electrochem Soc 149:E433
16. Mueller JT, Urban PM (1998) J Power Sources 75:39
17. Gileadi E (1993) In: Electrode kinetics for chemists, chemical engineers, and materials scientists. VCH Publishers, Inc., New York
18. Lefebvre MC, Martin RB, Pickup PG (1999) Electrochem Solid-State Lett 2:259
19. Li G, Pickup PG (2003) J Electrochem Soc 150:C745
20. Makharia R, Mathias MF, Baker DR (2005) J Electrochem Soc 152:A970
21. Guo JW, Zhao TS, Prabhuram J, Chen R, Wong CW (2005) Electrochim Acta 51:754
22. Bard AJ, Parsons R, Jordan J (eds) (1985) In: Standard potentials in aqueous solution. Marcel Dekker, New York
23. Havránek A, Klafki K, Wippermann K (2001) In: Büchi FN, Scherer GS, Wokaun A (eds) Proceedings of the First European polymer Electrolyte Fuel Cell forum, European Fuel Cell Forum, Oberrohrdorf, Switzerland, p 221
24. Havránek A, Wippermann K (2004) J Electroanal Chem 567:305
25. Eikerling M, Kornyshev AA (1999) J Electroanal Chem 475:107
26. Cole KS, Cole RH (1941) J Chem Phys 9:341
27. Lasia A (1999) In: Conway BE, White RE (eds) Modern aspects of electrochemistry. Kluwer/Plenum, New York, pp 32–143
28. Freire TJP, Gonzalez ER (2001) J Electroanal Chem 503:57
29. Boyer C, Gamburzev S, Velev O, Srinivasan S, Appleby AJ (1998) Electrochim Acta 43:3703
30. Kim J-H, Ha HY, Oh I-H, Hong S-A, Kim HN, Lee HI (2004) Electrochim Acta 50:801
31. Thomas SC, Ren X, Gottesfeld S (1999) J Electrochem Soc 146:4354
32. Sasikumar G, Ihm JW, Ryu H (2004) J Power Sources 132:11